Journal of Quality Measurement and Analysis *JQMA* 14(1) 2018, 101-113
Jurnal Pengukuran Kualiti dan Analisis

PERISTALTIC TRANSPORT OF BLOOD IN TERMS OF CASSON FLUID MODEL THROUGH A TUBE UNDER IMPACT OF MAGNETIC FIELD FOR MODERATE REYNOLDS NUMBER

(Pengangkutan Peristalsis Darah dalam Bentuk Model Bendalir Casson Melalui Tiub dengan Impak Medan Magnet bagi Nombor Reynolds Sederhana)

BILAL AHMED, TARIQ JAVED & MUHAMMAD SAJID

ABSTRACT

The effect of moderate non-zero Reynolds number on the nonlinear peristaltic transport of a blood flow through narrow arteries, where blood flow behaves similarly as a Casson fluid under the externally applied uniform magnetic field is investigated numerically. The governing equations for blood flow model of Casson fluid are formulated to a system of nonlinear coupled partial differential equations, which are exposed to Galerkin's finite element method. The assumptions of lubrication theory are neglected, due to which the effects of moderate Reynolds number and wave number along with other parameters are presented. To ensure the accuracy of developed code, obtained results are compared to that of available results in the literature and found in excellent agreement. The analysis shows that increasing Reynolds and Hartmann numbers enhance the velocity of the fluid. One of the findings of this study is the nonlinear behavior of pressure rise for large values of Reynolds and Hartmann numbers. Increasing wave number enhances the pressure rise in the peristaltic pumping region. The study also discussed to effect of Casson fluid parameter and time mean flow through graphs of velocity, pressure rise and contours of streamlines.

Keywords: peristaltic flow; blood flow Casson fluid model; magnetohydrodynamics; finite element method.

ABSTRAK

Kesan nombor Reynolds sederhana tak sifar terhadap pengangkutan peristalsis tak linear bagi aliran darah melalui arteri sempit yang tingkah laku aliran darah menyerupai bendalir Casson di bawah medan magnet seragam luaran, telah dikaji secara berangka. Persamaan menakluk bagi model aliran darah bendalir Casson diformulasi kepada suatu sistem persamaan pembezaan separa terganding tak linear, yang diselesaikan dengan kaedah unsur terhingga Galerkin. Andaian bagi teori pelinciran diabaikan, yang kesan nombor Reynolds sederhana dan nombor gelombang bersama parameter lain dipersembahkan. Bagi memastikan ketepatan kod berangka yang dibangunkan, keputusan yang terhasil dibandingkan dengan keputusan yang ada daripada kajian lepas dan didapati hasil bandingan adalah sangat baik. Analisis menunjukkan peningkatan nombor Reynolds dan nombor Hartmann meningkatkan halaju bendalir. Satu daripada penemuan kajian ini adalah tingkah laku tak linear kenaikan tekanan bagi nilai nombor Reynolds dan nombor Hartmann yang besar. Peningkatan nombor gelombang meningkatkan kenaikan tekanan dalam kawasan pengepaman peristalsis. Dalam kajian ini juga dibincangkan kesan parameter bendalir Casson dan aliran min masa melalui graf halaju, kenaikan tekanan dan kontur garis strim.

Kata kunci: aliran peristalsis; model aliran darah bendalir Casson; magnetohidrodinamik; kaedah unsur terhingga

1. Introduction

The circumferential progressive wave of either expansion or contraction generated along the tube is known as a mechanism of peristalsis. Peristalsis can be found in several organisms, in a variety of organs and in a number of industrial processes. Peristalsis is now getting more interest by engineers, a scientist as well as the researchers of biomedical sciences due to its vast applications in transporting of fluids. Physiologists considered peristalsis as one of the key mechanism of fluid transportation in biological systems. It includes transportation/ movement of urine in a body, movement of chime, transportation of spermatozoa in the cervical canal, vasomotion in small blood vessels and in the movement of lymph in the lymphatic vessels. The study of peristaltic flows give more effective mechanism for transporting in a sanitary fluid, industrial peristaltic pumping and in preparation of medical devices. In the printing industry, transporting of viscous fluids in mechanical roller pump and shifting of noxious fluids are good examples of peristaltic flows. Nowadays, many medical devices are manufactured on the basis of peristaltic mechanism to transport fluid without moving internal machinery parts such as heart-lung machine and dialysis system etc.

For quite some time, mechanism of peristalsis for mechanical as well as physiological research has become the major core of subject of scientific research. The first investigation was provided by Latham (1966). After him, several theoretical and experimental efforts are made to understand the peristalsis, so can apply practically more efficiently. The earliest and pioneer studies by Shapiro (1967), Fung and Yih (1968) and Shapiro *et al*. (1969) presented the phenomenon of peristalsis in the two-dimensional channel by an infinite wave of sinusoidal nature, this thus gives only qualitative relation by the ureter. These models also contain the explanation of biological and medical phenomena of reflux. Later, Weinberg *et. al.* (1971) and Lykoudis (1971) presented few more peristaltic models of ureteral waves. Fung (1971) studied the effect of coupling forces dynamics involving in ureteral muscle and functioning of the fluid mechanical organ. But the study of the peristaltic mechanism is not only important for ureteral physiology in the field of biosciences. One can find a number of investigations in which blood and other physiological fluid assumed to act like Newtonian fluids. But recently it has been found that most of the times physiological fluids show the properties of non-Newtonian fluids. The first comprehensive numerical approach about the peristaltic mechanism in the channel was given in Takabatake and Ayukawa (1982) and later Takabatake *et al.* (1988) provide results for two-dimensional peristaltic flow in the tube. The finite difference technique based on SOR method is applied in both studies to predict the characteristics of peristaltic flow for the ratio of wave amplitude and width of the channel for moderate Reynolds number and argued on the limitations of Jaffrin (1973) and Burns and Parkes (1967) perturbation results. They also concluded that in a cylindrical tube, peristaltic transport and mixing is greater as compared to that of the plane channel, and turbulence in the flow occurs when Reynolds number becomes greater than 2, while backward flow with trapping bolus exists at comparatively high values of Reynolds number for flow in the channel. The finite element technique is used by Takabatake *et al.* (1989) to study the peristaltic transport in the two-dimensional channel and presented the remarkable increasing effect of large wall slope at zero time mean flow on pressure rise.

The plasma shows the Newtonian fluid behavior while blood shows non-Newtonian behavior given in Johnston *et al.* (2004). At low shear rates, blood shows non-Newtonian behavior in small arteries but in large arteries at high shear rates, it behaves as Newtonian given in Rathod and Tanveer (2009). When blood flows through narrow arteries at a low shear rate, it behaves like a Casson fluid given in Sankar (2009), Srivastava and Srivastava (2009), and Nagarani *et al.* (2006). In narrow arteries with a diameter of $130 - 1000\ \mu m$,

Casson fluid is useful to consider it as a blood flow model given in Merill *et al.* (1965) and Venkatesan *et al.* (2013). But on reviewing the literature, it is evident that no rigorous effort has been made to present the transport of the fluid of non-Newtonian category in case of a small amplitude of wave before Raju and Deventhan (1972). Srivastava and Srivastava (1984) investigated blood transportation by ignoring peripheral layer which allows blood to behave as single layered Casson fluid. Later, Srivastava (1987) presented the study for the axisymmetric flow of Casson fluid in a circular tube. Das and Batara (1993) investigated the fully developed model of Casson fluid for steady flow passing through the tube at low Dean number. Elshehawey *et al.* (1998) presented peristaltic transport model of Carreu fluid in a channel with the assumption of long wavelength and low Reynolds number. Some recent studies related to peristaltic motion and other flow model under the influence of magnetic field and other physical situations are found in literature (Siddiqui & Schwarz 1994; Kumar & Naidu 1995; Khan *et al.* 2018; Hayat *et al.* 2018). Khan *et al.* (2017a) gave a comparison of Casson fluid with homogeneous/heterogeneous reactions. Khan *et al.* (2017b) extended the work presented in (2017a) and investigated the stagnation point flow of Casson fluid over a stretching sheet with homogeneous/heterogeneous reactions. The flow of Casson fluid over a stretching cylinder under the influence of magnetic field was investigated by Tamoor *et al.* (2017). The effects of the non-orthogonal inclined magnetic field on the flow of micropolar Casson fluid was studied by Iqbal *et al.* (2017) using the Keller box scheme.

Motivated by above-mentioned studies, the present investigation is carried out in the viewing of the fact that long wavelength and low Reynolds number assumptions buried many aspects of the peristaltic motion. So, in this study, the mathematical modelling and simulation of peristaltic transportation of the Casson fluid passing through the tube under the influence of magnetic field without implementation of the assumptions of lubrication theory i.e. the assumptions of long wavelength and low Reynolds number is presented, which allows to predict the effects of dominant inertial forces and wave number which are not yet discussed in the literature. By dropping such assumptions our model becomes a system of non-linear partial differential equations. An efficient technique based on Galerkin's formulation finite element method is used to obtain the numerical results for velocity, pressure and stream function along with vorticity for different variations of other parameters and Reynolds number are presented the first time in literature. The obtained results are also deduced to lubrication theory, and hence validated and found in good agreement.

2. Mathematical Modeling

Consider the peristaltic transport of an electrically conducting Casson fluid motion of blood flow passing through a horizontal tube of width $2a$. Peristaltic tube is subject to the influence of applied magnetic field of uniform strength B_0 perpendicular to the direction of the flow. Here, due to small conductivity of fluid, the low magnetic Reynolds number R_m-approximation is assumed which allows to neglect induced magnetic field caused by applied magnetic field. Unsteady flow is considered with constant thermos-physical properties in which flow is caused by peristaltic walls along $z-$direction and $r-$direction is taken along radial direction. The symmetry of the peristaltic flow is about z-direction and schematic of the flow is presented in Figure 1. The peristaltic walls of tube moves and follows the relation given as

$$H(Z,t) = a - b\cos\left[\frac{2\pi}{\lambda}(Z - ct)\right], \tag{1}$$

where b, λ and c are wave amplitude, wavelength and speed of the flow respectively.

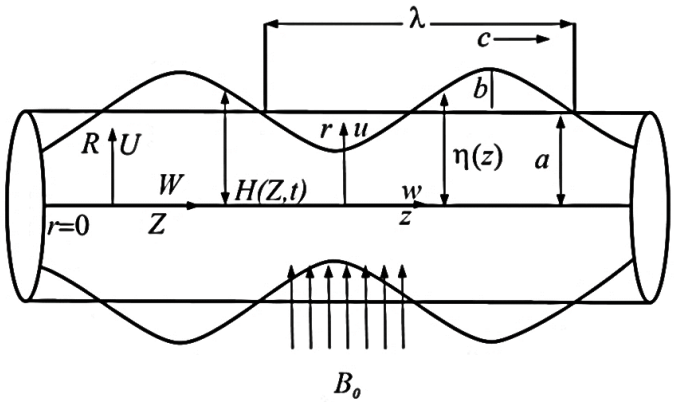

Figure 1: Geometrical flow diagram

The governing equations that describe the flow of Casson fluid in a tube under the influence of magnetic effects appeared through Lorentz force term are partial differential equations as follows:

$$\frac{\partial W}{\partial Z}+\frac{1}{R}\frac{\partial (RU)}{\partial R}=0, \tag{2}$$

$$\rho\left(\frac{\partial W}{\partial t}+W\frac{\partial W}{\partial Z}+U\frac{\partial W}{\partial R}\right)=-\frac{\partial P}{\partial Z}+\mu\left(1+\frac{1}{\beta}\right)\frac{1}{R}\frac{\partial}{\partial R}\left(R\frac{\partial W}{\partial R}\right)+\frac{\partial^2 W}{\partial Z^2}-\sigma B_0^2 W, \tag{3}$$

$$\rho\left(\frac{\partial U}{\partial t}+W\frac{\partial U}{\partial Z}+U\frac{\partial U}{\partial R}\right)=-\frac{\partial P}{\partial R}+\mu\left(1+\frac{1}{\beta}\right)\frac{\partial}{\partial R}\left(\frac{1}{R}\frac{\partial (RU)}{\partial R}\right)+\frac{\partial^2 U}{\partial Z^2}, \tag{4}$$

where ρ is the density, μ is the viscosity and β is the Casson fluid parameter. Casson fluid is basically shear thinning fluid which holds the property that it at zero shear rate Casson fluid attains infinite viscosity and consequently below yield stress by which no flow occurs and on the other hand Casson fluid have zero viscosity at infinite shear rate by which fluid model reduces to a model for Newtonian fluid. The suitable boundary conditions that assist the discussed flow are given as

$$\frac{\partial W}{\partial R}=0,\quad U=0\quad \text{at}\quad R=0\ \text{and}\ W=0,\quad U=\frac{\partial H}{\partial t}\quad \text{at}\quad R=H. \tag{5}$$

The defined boundary condition in Eq. (5) on W at $R=0$ corresponds to symmetry of flow and $R=H$ corresponds to no-slip of the wall. While the defined boundary condition on U at $R=H$ as $U=\partial H/\partial t$ reflects that the velocity of fluid is equal to the velocity of the wall. At center of the tube, transverse velocity is zero so that we have boundary condition at $R=0$ as $U=0$. The conversion relation between the lab and wave frame of reference given in Siddiqui and Schwarz (1994) are

$$w^*=W-c,\qquad u^*=U,\qquad z^*=Z-ct,\qquad r^*=R, \tag{6}$$

where z^*, r^* and Z, R represent the velocity components in moving and fixed frame respectively. After incorporating the above transformation in Eqs. (2) to (4), we get

$$\frac{1}{r^*}\frac{\partial (r^*u^*)}{\partial r^*}+\frac{\partial w^*}{\partial z^*}=0, \tag{7}$$

$$\rho\left(w^*\frac{\partial w^*}{\partial z^*}+u^*\frac{\partial w^*}{\partial r^*}\right)=-\frac{\partial p^*}{\partial z^*}+\mu\left(1+\frac{1}{\beta}\right)\frac{1}{r^*}\frac{\partial}{\partial r^*}\left(r^*\frac{\partial w^*}{\partial r^*}\right)+\frac{\partial^2 w^*}{\partial z^{*2}}-\sigma B_0^2(w^*+c), \tag{8}$$

$$\rho\left(w^*\frac{\partial u^*}{\partial z^*}+u^*\frac{\partial u^*}{\partial r^*}\right)=-\frac{\partial p^*}{\partial r^*}+\mu\left(1+\frac{1}{\beta}\right)\frac{\partial}{\partial r^*}\left(\frac{1}{r^*}\frac{\partial (r^*u)}{\partial r^*}\right)+\frac{\partial^2 u^*}{\partial z^{*2}}. \tag{9}$$

Introducing the following dimensionless variables to the system of equations

$$\left.\begin{aligned} w=\frac{w^*}{c}, u=\frac{u^*}{c}\ z=\frac{z^*}{\lambda}, r=\frac{r^*}{a}, \alpha=\frac{a}{\lambda}, \phi=\frac{b}{a}, \psi=\frac{\psi^*}{ca}, \omega=\frac{\omega^*}{c/a}, \\ p=\frac{a^2}{\lambda\mu c}p^*(z), q=\frac{q^*}{ca}, \eta=\frac{\eta^*}{a}, h=\frac{h(x^*)}{a}, Re=\frac{ca}{\nu}\alpha, M=\sqrt{\frac{\sigma}{\mu}}B_0 a \end{aligned}\right\}. \tag{10}$$

The associated boundary conditions (Kumar & Naidu 1995) for the flow at center and wall of the tube are given by

$$\psi^*=0 \text{ at } r^*=0 \text{ and } \psi^*=q^* \text{ at } r=\eta(z^*), \tag{11}$$

where ψ^* represents stream function and rates in the wave frame are related by the expression $q^*=Q^*-cH^2$ with the time mean flow in the laboratory frame Q^*. Eliminating pressure gradient term by cross differentiation, and by introducing the relations $u=-\frac{\alpha}{r}\partial\psi/\partial z$ and $w=\frac{1}{r}\partial\psi/\partial r$, the governing equations for the considered flow formulation are as follows:

$$\frac{\alpha^2}{r}\frac{\partial^2\psi}{\partial z^2}+\frac{\partial}{\partial r}\left(\frac{1}{r}\frac{\partial\psi}{\partial r}\right)=-\omega, \tag{12}$$

$$Re\left(\frac{\partial\psi}{\partial r}\frac{\partial}{\partial z}\left(\frac{\omega}{r}\right)-\frac{\partial\psi}{\partial z}\frac{\partial}{\partial r}\left(\frac{\omega}{r}\right)\right)=\left(1+\frac{1}{\beta}\right)\frac{1}{r}\mathrm{D}^2(r\omega)+M^2\frac{\partial}{\partial r}\left(\frac{1}{r}\frac{\partial\psi}{\partial r}\right), \tag{13}$$

where Re is Reynolds number and M is Hartmann number. Modified form of Laplacian operator D^2 is defined as $\mathrm{D}^2=\alpha^2\frac{\partial^2}{\partial z^2}+\frac{\partial^2}{\partial r^2}-\frac{1}{r}\frac{\partial}{\partial r}$ and boundary conditions yield the form as

$$\left.\begin{aligned} \psi=0,\ \ \frac{\partial}{\partial r}\left(\frac{1}{r}\frac{\partial\psi}{\partial r}\right)=0,\ \ \frac{1}{r}\frac{\partial\psi}{\partial z}=0 \qquad \text{at}\quad r=0 \\ \psi=q,\ \ \frac{1}{r}\frac{\partial\psi}{\partial r}=-1,\quad \frac{1}{r}\frac{\partial\psi}{\partial z}=2\pi\phi\sin 2\pi z \quad \text{at}\quad r=\eta(z) \end{aligned}\right\}. \tag{14}$$

At the center of the tube $z=0$, pressure rise per wavelength is defined in wave frame as

$$\Delta p_\lambda=\int_0^\lambda\frac{\partial p}{\partial z}dz. \tag{15}$$

3. Numerical Analysis

In the present analysis, the governing equations are obtained by dropping the assumptions of lubrication theory i.e. long wavelength and low Reynolds number. So, we have set of coupled partial differential equations which are solved numerically by using finite element method based on Galerkin's formulation. We discretize the considered domain into a mesh of triangular elements contains six nodes per element. The solution of each triangular mesh is found and assemble all solution to form a global system. Finally, the solution has been obtained by using the Newton-Raphson method. In all cases, highly convergent results are obtained by our own built MATLAB code with a tolerance of 10^{-14} in $3-5$ iterations.

The stream function ψ and vorticity ω is approximated by the following approximation

$$\psi=\sum_{k=1}^{n}N_k\psi_k,\quad \omega=\sum_{k=1}^{n}N_k\omega_k, \tag{16}$$

where ψ_k and ω_k are nodal element approximation of ψ and ω respectively. Galerkin's finite element approach turns Eqs. (12) and (13) as

$$\int_\Omega w_1\left(\frac{\alpha^2}{r}\frac{\partial^2\psi}{\partial z^2}+\frac{\partial}{\partial r}\left(\frac{1}{r}\frac{\partial\psi}{\partial r}\right)+\omega\right)d\Omega=0, \tag{17}$$

$$\int_\Omega w_2\left(Re\left(\frac{\partial\psi}{\partial r}\frac{\partial}{\partial z}\left(\frac{\omega}{r}\right)-\frac{\partial\psi}{\partial z}\frac{\partial}{\partial r}\left(\frac{\omega}{r}\right)\right)-M^2\frac{\partial}{\partial r}\left(\frac{1}{r}\frac{\partial\psi}{\partial r}\right)-\left(1+\frac{1}{\beta}\right)\frac{1}{r}\mathrm{D}^2(r\omega)\right)d\Omega=0, \tag{18}$$

in which w_1 and w_2 are weight functions and $d\Omega=2\pi r dr dz$. Simplification of Eqs. (17) and (18) yields

$$\int_\Omega \left(\frac{\alpha^2}{r}\frac{\partial w_1}{\partial z}\frac{\partial \psi}{\partial z}+\frac{\partial w_1}{\partial r}\left(\frac{1}{r}\frac{\partial \psi}{\partial r}\right)-w_1\omega\right)d\Omega=\int_\Gamma\ w_1\frac{\partial \psi}{\partial n}d\Gamma \tag{19}$$

$$\int_\Omega\ w_2\,Re\left(\frac{\partial \psi}{\partial r}\frac{\partial}{\partial z}\left(\frac{\omega}{r}\right)-\frac{\partial \psi}{\partial z}\frac{\partial}{\partial r}\left(\frac{\omega}{r}\right)\right)d\Omega+\left(1+\frac{1}{\beta}\right)\int_\Omega\left(\frac{\partial w_2}{\partial r}\frac{1}{r}\frac{\partial(r\omega)}{\partial r}+\frac{\alpha^2}{r}\frac{\partial w_2}{\partial z}\frac{\partial(r\omega)}{\partial z}\right)d\Omega\ +M^2\int_\Omega\left(\frac{\partial w_2}{\partial r}\frac{1}{r}\frac{\partial \psi}{\partial r}\right)d\Omega=\left(1+\frac{1}{\beta}\right)\int_\Gamma\ w_2\frac{\partial(r\omega)}{\partial n}d\Gamma+M^2\int_\Gamma\ w_2\frac{\partial \psi}{\partial n}d\Gamma, \tag{20}$$

where $d\Gamma$ is defined as $d\Gamma=\pi r dr dz$. Introducing approximations defined in Eq. (16) into Eqs. (19) and (20) and after discretizing the domain, we get

$$-\sum_i B^e_{ki}\omega_i+\sum_i A^e_{ki}\psi_i\ =S^{k^e}_n, \tag{21}$$

$$Re\sum_i C^e_{kij}\psi_i\omega_i+\left(1+\frac{1}{\beta}\right)\sum_i A^e_{ki}\omega_i+M^2\sum_i D^e_{ki}\psi_i\ =M^2S^{k^e}_n. \tag{22}$$

where

$$A^e_{ki}=\int_{\Omega^e}\left(\frac{\alpha^2}{r}\frac{\partial N_k}{\partial z}\frac{\partial N_i}{\partial z}+\frac{\partial N_k}{\partial r}\left(\frac{1}{r}\frac{\partial N_i}{\partial r}\right)\right)d\Omega, \tag{23}$$

$$B^e_{ki}=\int_{\Omega^e}N_kN_i d\Omega, \tag{24}$$

$$C^e_{kij}=\int_\Omega\ N_k\left(\frac{\partial N_i}{\partial r}\frac{\partial}{\partial z}\left(\frac{N_j}{r}\right)-\frac{\partial N_j}{\partial z}\frac{\partial}{\partial r}\left(\frac{N_i}{r}\right)\right)d\Omega, \tag{25}$$

$$D^e_{ki}=\int_\Omega\left(\frac{\partial N_k}{\partial r}\frac{1}{r}\frac{\partial N_k}{\partial r}\right)d\Omega, \tag{26}$$

$$S^{k^e}_n=\int_\Gamma\ N_k\overline{S}_k d\Gamma, \tag{27}$$

The global system in matrix form is defined as

$$\boldsymbol{KA}=\boldsymbol{F}, \tag{28}$$

where

$$K_{ij}=\begin{bmatrix}-B^e_{ki} & A^e_{ki}\\ \left(1+\frac{1}{\beta}\right)A^e_{ki} & ReC^e_{kij}\omega_i+M^2D^e_{ki}\end{bmatrix}, A_k=\begin{bmatrix}\omega_k\\ \psi_k\end{bmatrix}, F_k=\begin{bmatrix}S^{k^e}_n\\ M^2S^{k^e}_n\end{bmatrix}. \tag{29}$$

4. Results and Discussion

The numerical scheme discussed in the previous section is implemented using MATLAB to obtain the graphs of velocity, pressure, contours of streamlines and vorticity. Influence of involved parameters like Reynolds number Re, amplitude ratio ϕ, wave number α, volume flow rate Q, Hartmann number M and Casson fluid parameter β on the quantities of the interest is presented graphically with detailed discussion.

4.1. *Validation*

This section is dedicated for authentication of our own build MATLAB code of finite element method which gives the numerical solution of a modeled system of nonlinear partial differential equations. Shapiro *et al.* (1969) give results of peristaltic transport by applying lubrication theory. These results are purely analytical and hence considered to be a benchmark solution in this comparison. The obtained results of pressure distribution are compared with

that of results given Shapiro *et al.* (1969) by plotting both results in Figure 2. The graphs presented in Figure 2 exhibits good agreement for $M = 0, 1/\beta = 0$ under assumption of long wavelength and low Reynolds number with corresponding results of Shapiro *et al.* (1969).

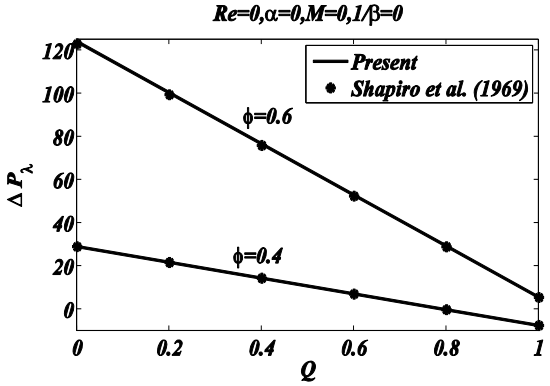

Figure 2: Comparison of computed pressure distribution with that of results provided by Shapiro *et al.* (1969)

4.2. *Velocity profile*

In this section, the behavior of longitudinal velocity at cross-section $z = 0$ is analyzed and discussed after plotting the graphs of Reynolds number Re, wave number α, Casson fluid parameter β, Hartmann number M and time mean flow for different set of parameters involved in the model. In Figure 3, the effect of different values of Hartmann number on the behavior of velocity for various values of Reynolds number is presented by plotting velocity profile against Reynolds number Re. We observe that increasing the Hartmann number enhances the velocity independent of the choice of the Reynolds number. It is also observed that maximum value is achieved at $Re = 99$ and solution remains smooth for large values of Reynolds number.

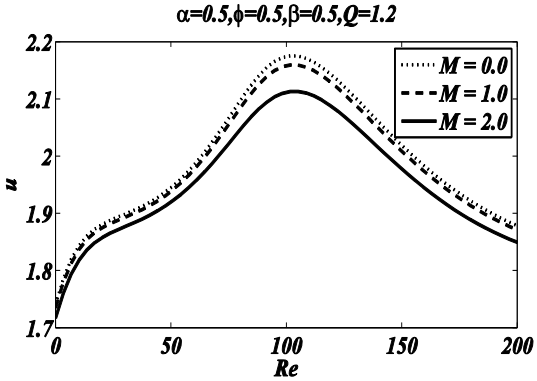

Figure 3: Variation of velocity distribution against Re for different M

The velocity field presented in Figure 4 exhibits that behavior of velocity in the central region of the tube and in the vicinity of peristaltic wall is not similar for cases of different Reynolds number Re Hartmann number M, wave number α and Casson fluid parameter β. In the literature, lubrication theory is widely used to study the peristaltic mechanism which is not able to predict the effects of inertial forces. The ratio of inertial forces to viscous forces corresponds to Reynolds number. The effects of different values of Reynolds number are shown in Figure 4(a). The increase in the Reynolds number relates to the dominance of inertial forces as compared to viscous forces which enhances the flow in the central region of

the tube but opposite effect is noticed in the vicinity of the peristaltic wall. These facts are reported first time for transportation of peristaltic motion of Casson fluid in a tube in any physical situation. Figure 4(b) is plotted for velocity profile to show the effects of different wave number. The ratio of the width of the tube to the wavelength is presented by wave number. Increasing wave number reduces the velocity in the center of the tube and a slight increase is noted near the walls of the tube. The viscosity of the Casson fluid is zero at an infinite shear rate and infinite at zero shear rate.

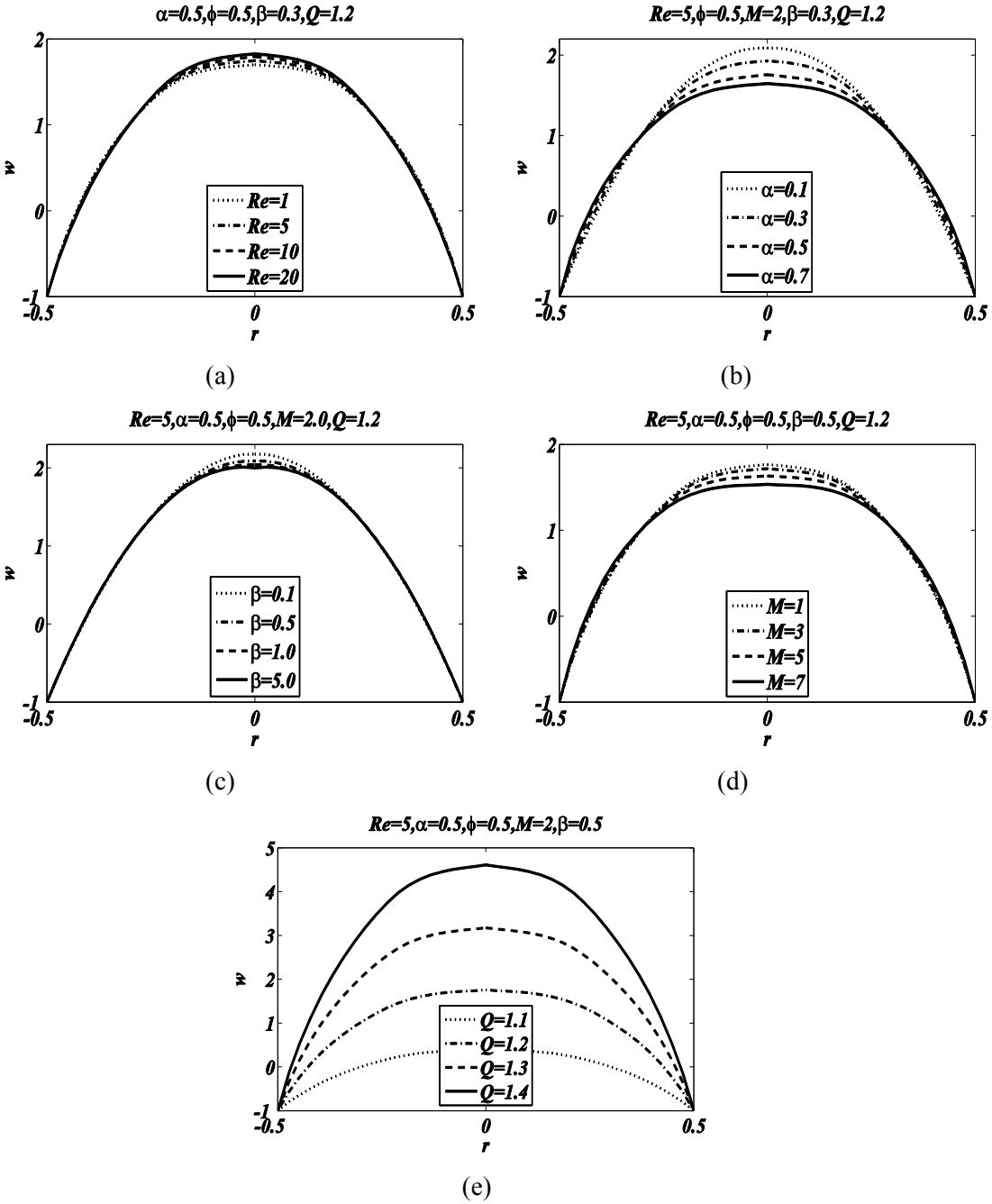

Figure 4: Longitudinal velocity distribution for different values of (a) Re, (b) α, (c) β , (d) M and (e) Q with fixed values of other parameters

The viscosity of the Casson fluid can be controlled by setting the Casson fluid parameter in different ranges. Figure 5(c) is presented to shown the effects of the Casson fluid parameter on the velocity profile which are as same as in the case of wave number. The Hartmann number corresponds to the ration of electromagnetic forces to viscous forces, so increasing the value of Hartmann number reflects the enhancement of electromagnetic forces which is caused by increasing the strength of magnetic field. The enhancement in the strength of the electromagnetic forces increases the velocity in the region near the peristaltic wall and causes resistance to the flow in the central region of the tube as shown in Figure 5(d). The effect of time means flow on the velocity of the Casson fluid is presented in Figure 5(e). It reveals that the behavior of time mean flow rate is quite different as compared to other participated parameters as it shows same behavior in both the central region of the tube and in the region near the walls of the tube. The increase in time-mean flow rate increases the longitudinal velocity of the fluid in the whole region of the tube.

4.3. *Pressure distribution*

This section is dedicated to detail discussion on the pressure of the peristaltic transportation of Casson fluid. The importance of Casson fluid of blood flow model is highly dependent on pressure rise per wavelength in narrow arteries where at low shear rates blood behaves like Casson fluid transport of Casson fluid of blood flow is presented in Figure 5.

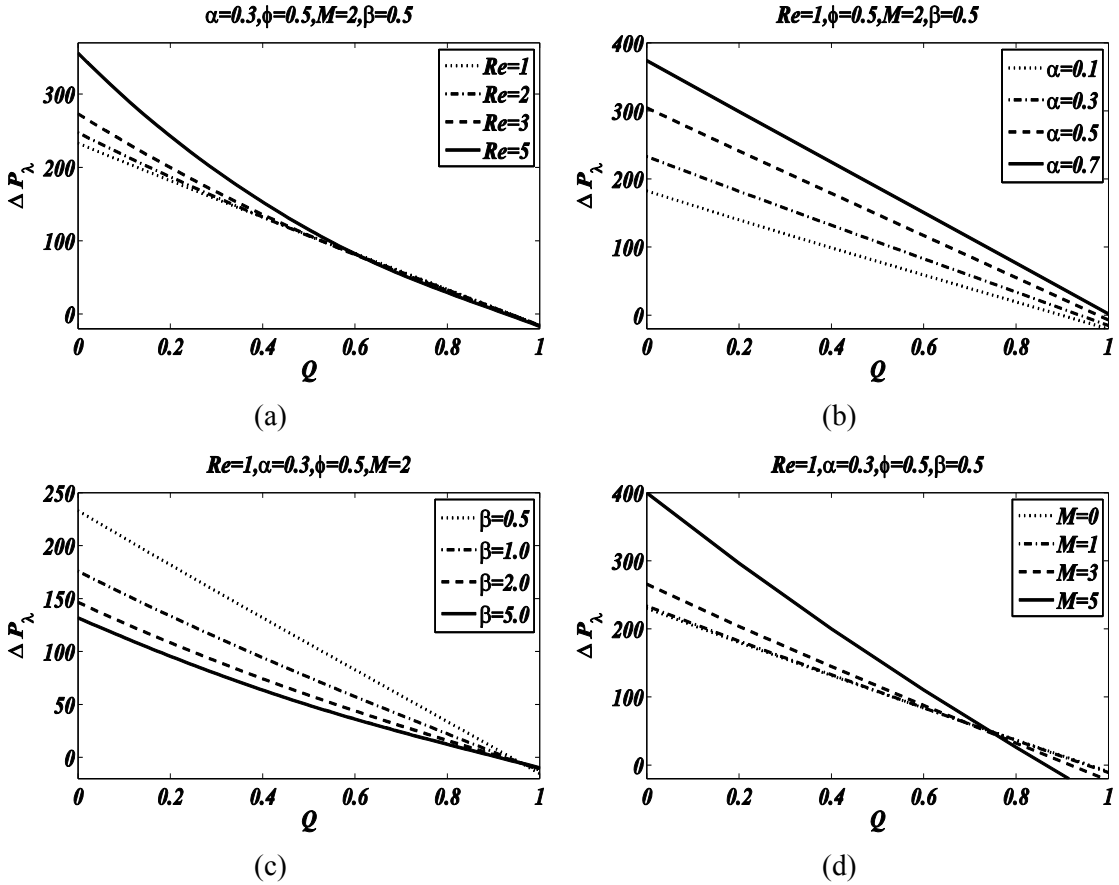

Figure 5: Pressure rise per wavelength for different values for (a) Re, (b) α, (c) β and (d) M, with fixed values of other parameters

Figure 5(a) reveals the effect of Reynolds number Re on pressure rise per wavelength. It is observed that for large values of Reynolds number, the rise in pressure shows non-linear behavior due to strong inertial forces. It is also noted that dominance of inertial forces to viscous forces causes augmentation in a rise in pressure and this fact is not reported in any previous study. Furthermore, increasing wave number α shows analogous behavior as to that of Reynolds number. The decrease in pressure rise in the pumping region is noticed due to increase in Casson fluid parameter β, because due to rise in viscosity, flow becomes slow and the pressure rise decreases. On the other hand, the increase in rise in pressure is noticed with increasing values of Hartmann number M. Usually, the three ranges of pumping in peristalsis are possible, for $\Delta P > 0$ corresponds to augmented pumping region while $\Delta P = 0$ is the free pumping region and $\Delta P < 0$ is the co-pumping region. We have presented only first to which are of most interest for engineering and have vastly applicable in bio-medical sciences. The pressure rise per wavelength in peristaltic So, one way to control the pressure rise of peristaltic motion of Casson fluid of blood flow by varying the strength of the applied magnetic field, this fact is widely used in MRI and other bio medical treatments. Figure 5(d) exhibits that in the region of augmented pumping $0.7 < Q < 1$, pressure rise shows opposite behavior as compared to that of pumping region corresponds to interval $0 < Q < 0.7$. Free pumping corresponds to the relation $\Delta P = 0$ at $Q = 0.7$.

4.4. *Trapping and vorticity*

Another important phenomenon of peristaltic motion is trapping which is basically due to the formation of bolus by internal circulation of streamlines. This physical phenomenon relates to thrombus formation of blood and motion of fluid bolus in the gastrointestinal tract. The trapping phenomena for variation of different parameters involved are presented in Figures 6 to 10. Figure 6 shows the contours of streamlines for different values of Reynolds number with $\alpha = 0.3, \phi = 0.5, M = 2.0, \beta = 0.5, Q = 1.2$. It shows that increase in Reynolds number magnifying the size of bolus as well as increases the number of bolus. In other words, the cluster of bolus can be shifted on right side of the tube by enhancing the inertial forces, by

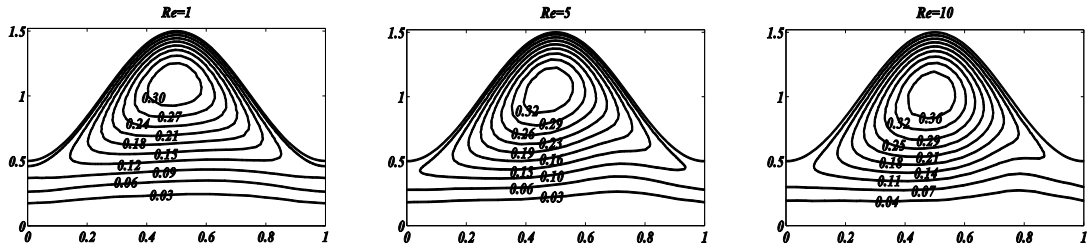

Figure 6: Contours of streamlines for $Re = 1$, 5 and 10 with fixed $\alpha = 0.1, \phi = 0.5, M = 2.0, \beta = 0.5, Q = 1.2$ in wave frame

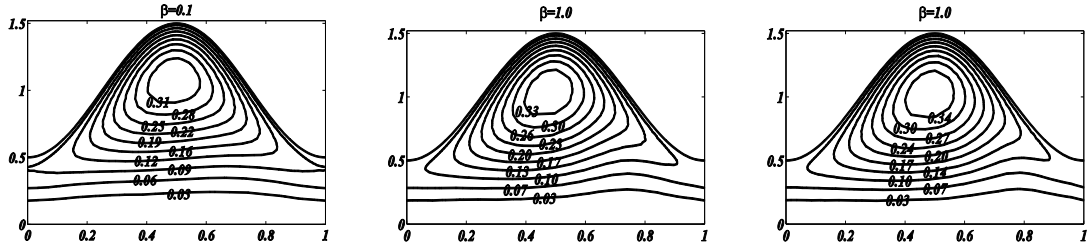

Figure 7: Contours of streamlines for $\beta = 0.1$ 1.0 and 5.0 with fixed $Re = 5, \alpha = 0.1, \phi = 0.5, M = 2.0, Q = 1.2$ in wave frame

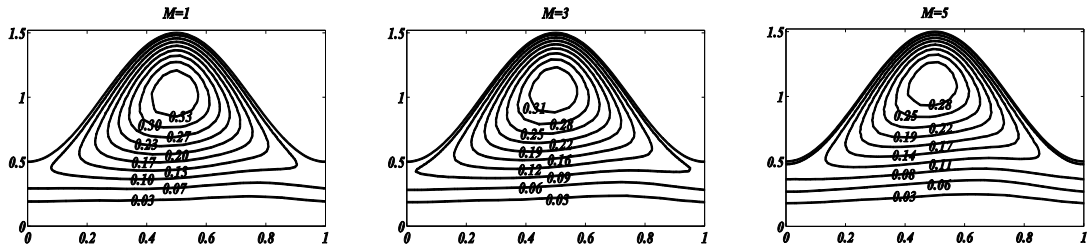

Figure 8: Contours of streamlines for $M = 1, 3$ and 5 with fixed $Re = 5.0, \alpha = 0.3, \phi = 0.5, \beta = 0.5, Q = 1.2$ in wave frame

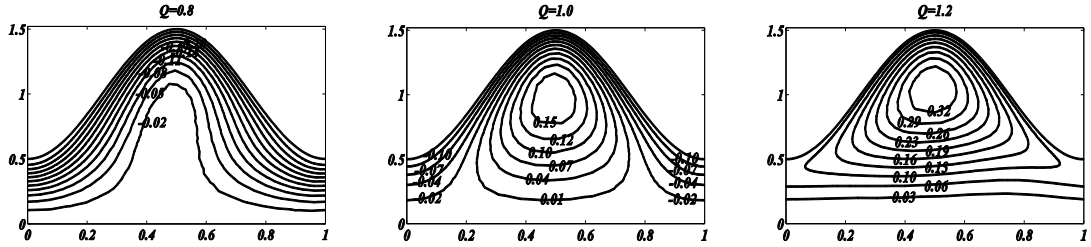

Figure 9: Contours of streamlines for $Q = 0.8$,1.0 and 1.2 with fixed $Re = 5.0, \alpha = 0.3, \phi = 0.5, M = 2.0, \beta = 0.5$ in wave frame

increasing Reynolds number. Figure 7 shows the variation of streamlines for different values of Casson fluid parameter β with $Re = 5, \alpha = 0.1, \phi = 0.5, M = 2.0, Q = 1.2$. The increase in number and size of bolus is noted as a result of increasing Casson fluid parameter. The effect of Hartmann number M on the streamlines are presented by plotting contours in Figure 8 with fixed $Re = 5.0, \alpha = 0.3, \phi = 0.5, \beta = 0.5, Q = 1.2$. The opposite behavior is noticed as in case of Casson fluid parameter. The contours of streamlines for various values of time mean flow rate Q are presented in Figure 9 with fixed values of other involved parameters i.e. $Re = 5.0, \alpha = 0.3, \phi = 0.5, M = 2.0, \beta = 0.5$. Figure 9 exhibits that the flow is generated and moves along the peristaltic wall for $Q < 1$ and streamlines of almost same trajectory of peristaltic wall are appeared, while for $Q = 1$ formation of bolus are found in crest region of the tube shows circulatory motion of the fluid and some streamlines still moves along the wall and obeys the same path in the vicinity of the peristaltic wall. The flow becomes smooth in the central region of the tube for $Q > 1$ with increase in bolus is noted The contours of vorticity for Re are presented in Figure 10 which exhibits that flow generates on the center of the tube and ends on the peristaltic wall and in the central region.

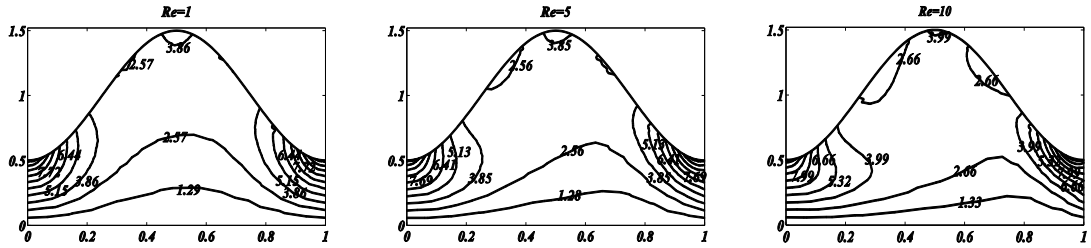

Figure 10: Contours of vortices for $Re = 1$ 5 and 10 with fixed $\alpha = 0.1, \phi = 0.5, M = 2.0, \beta = 0.5, Q = 1.2$ in wave frame

5. Conclusion

The effect of Reynolds number on a peristaltic transportation of non-Newtonian behavior of blood has been investigated by considering blood as a Casson fluid. The governing equations are developed and modeled by dropping the long wavelength and low Reynolds number which allow us to predict the features of peristaltic motion for moderate values of Reynolds number and wave number. The flow is subjected to the external uniform magnetic field to observe the effect of Hartmann number in different situations. Finite element method is used to solve modeled set of coupled partial differential equations. The investigation found that the velocity shows opposite behavior at the central region of the tube and near the wall. It is concluded that increasing values Reynolds number enhances velocity at the center of the tube, while opposite behavior is observed for increasing wave number. The same opposite behavior is also observed in case of Casson fluid parameter and Hartmann number. Unlikely to other parameters, time mean flow rate effects the velocity with the same attitude through the whole region. Pressure rise per wavelength is decreased by increasing Casson flow parameter. Opposite effects are noticed for Reynolds number and wave number while for high values of Reynolds number, pressure rise per wavelength exhibits nonlinear behavior. The increasing values of Hartman number ensure strengthen of electromagnetic forces as compared to viscous forces that cause the reduction in size and number of trapping bolus. The increase in Casson flow parameter enhances the thickness of fluid and caused reduction of size and number of the bolus. The dominate inertial forces caused by an increase in Reynolds number increases the magnitude and number of trapped bolus and vorticity exhibit the generation of the flow field in the narrow part of the tube in this case. First time in literature, this study includes the solution of the full form of Navier-Stokes equations for the peristaltic motion for Casson fluid passing through a tube filled with the porous medium in a magnetic field. Hence, it is hoped that present study serves as a benchmark for further research on peristaltic flows of non-Newtonian fluids without applying assumption of lubrication theory.

References

Burns J.C. & Parkes T. 1967. Peristaltic motion. *Journal of Fluid Mechanics* **29**(4): 731-743.

Das B. & Batra R.L. 1993. Secondary flow of a Casson fluid in a slightly curved tube. *International Journal of Non-Linear Mechanics* **28**(5): 567-577.

Elshehawey E.F., El Misery A.E.M. & El Hakeem Abd El Naby A. 1998. Peristaltic motion of generalized Newtonian fluid in a non-uniform channel. *Journal of the Physical Society of Japan* **67**(2): 434-440.

Fung Y.C.B. 1971. Peristaltic pumping: a bioengineering model. In *Urodynamics*: 177-198.

Fung Y.C. & Yih C.S. 1968. Peristaltic transport. *Journal of Applied Mechanics* **35**(4): 669-675.

Hayat T., Qayyum S., Khan M.I. & Alsaedi A. 2018. Entropy generation in magnetohydrodynamic radiative flow due to rotating disk in presence of viscous dissipation and Joule heating. *Physics of Fluids* **30**(1): 017101.

Iqbal Z., Mehmood R., Azhar E. & Mehmood Z. 2017. Impact of inclined magnetic field on micropolar Casson fluid using Keller box algorithm. *The European Physical Journal Plus* **132**(4): 175.

Jaffrin M.Y. 1973. Inertia and streamline curvature effects on peristaltic pumping. *International Journal of Engineering Science* **11**(6): 681-699.

Johnston B., Johnston P., Corney S. & Kilpatrick D. 2004. Non-Newtonian blood flow in human right coronary arteries: steady state simulations. *Journal of Biomechanics* **37**: 709–720.

Khan M.I., Qayyum S., Hayat T., Waqas M., Khan M.I. & Alsaedi A. 2018. Entropy generation minimization and binary chemical reaction with Arrhenius activation energy in MHD radiative flow of nanomaterial. *Journal of Molecular Liquids* **259**: 274-283.

Khan M.I., Waqas M., Hayat T. & Alsaedi A. 2017. A comparative study of Casson fluid with homogeneous-heterogeneous reactions. *Journal of Colloid and Interface Science* **498:** 85-90.

Khan M.I., Waqas M., Hayat T. & Alsaedi A. 2017. Magnetohydrodynamic (MHD) stagnation point flow of Casson fluid over a stretched surface with homogeneous–heterogeneous reactions. *Journal of Theoretical and Computational Chemistry* **16**(3): 1750022.

Kumar B.R. & Naidu K.B. 1995. A numerical study of peristaltic flows. *Computers & Fluids* **24**(2): 161-176.

Latham T.W. 1966. Fluid motions in a peristaltic pump. PhD Thesis. Massachusetts Institute of Technology.

Lykoudis P.S. 1971. Peristaltic pumping: A bioengineering model. *Proceedings of the Workshop in Hydrodynamic Upper Urinary Tract, Nat. Acad. Sci., Washington, DC*.

Merrill E.W., Benis A.M., Gilliland E.R., Sherwood T.K. & Salzman E.W. 1965. Pressure-flow relations of human blood in hollow fibers at low flow rates. *Journal of Applied Physiology* **20**(5): 954-967.

Nagarani P., Sarojamma G. & Jayaraman G. 2006. Exact analysis of unsteady convective diffusion in Casson fluid flow in an annulus–Application to catheterized artery. *Acta Mechanica* **187**(1-4): 189-202.

Raju K.K. & Devanathan R. 1972. Peristaltic motion of a non-Newtonian fluid. *Rheologica Acta* **11**(2):170-178.

Rathod V.P. & Tanveer S. 2009. Pulsatile flow of couple stress fluid through a porous medium with periodic body acceleration and magnetic field. *Bulletin of the Malaysian Mathematical Sciences Society* **32**(2): 245–259.

Sankar D.S. 2009. Two-fluid flow of blood through asymmetric and axisymmetric stenosed narrow arteries. *International Journal of Nonlinear Sciences and Numerical Simulation* **10**(11-12): 1425-1442.

Shapiro A.H. 1967. Pumping and retrograde diffusion in peristaltic waves. *Proceedings of the Workshop in Ureteral Reflux in Children*, pp. 109-126.

Shapiro A.H., Jaffrin M.Y. & Weinberg S.L. 1969. Peristaltic pumping with long wavelengths at low Reynolds number. *Journal of Fluid Mechanics* **37**(4): 799-825.

Siddiqui A.M. & Schwarz W.H. 1994. Peristaltic flow of a second-order fluid in tubes. *Journal of Non-Newtonian Fluid Mechanics* **53:** 257-284.

Srivastava L.M. 1987. Peristaltic transport of a Casson fluid. *Nigerian Journal of Scientific Research* **1**: 71-82.

Srivastava L.M. & Srivastava V.P. 1984. Peristaltic transport of blood: Casson model—II. *Journal of Biomechanics* **17**(11): 821-829.

Takabatake S. & Ayukawa K. 1982. Numerical study of two-dimensional peristaltic flows. *Journal of Fluid Mechanics* **122**: 439-465.

Takabatake S., Ayukawa K. & Mori A. 1988. Peristaltic pumping in circular cylindrical tubes: a numerical study of fluid transport and its efficiency. *Journal of Fluid Mechanics* **193**: 267-283.

Takabatake S., Ayukawa K. & Sawa M. 1989. Finite Element Analysis of Two-dimensional Peristaltic Flow (1st Report, Finite element solution). *Japan Society of Mechanical Engineering* **53**: 1207-1213.

Tamoor M., Waqas M., Khan M.I., Alsaedi A. & Hayat T. 2017. Magnetohydrodynamic flow of Casson fluid over a stretching cylinder. *Results in Physics* **7**: 498-502.

Venkatesan J., Sankar D.S., Hemalatha K. & Yatim Y. 2013. Mathematical analysis of Casson fluid model for blood rheology in stenosed narrow arteries. *Journal of Applied Mathematics* **2013**: 583809 (11 pages).

Weinberg S.L., Jaffrin M.Y. & Shapiro A.H. 1971. Hydrodynamic model of ureteral function. In *Urodynamics*: 217-231.

Department of Mathematics and Statistics
International Islamic University
H-10, Islamabad, 44000, PAKISTAN
E-mail: bilalmaths7@yahoo.com, tariq_17pk@yahoo.com, sajidqau2002@yahoo.com*

*Corresponding author